Effect of initial conformation, flow strength, and hydrodynamic interaction on polymer molecules in extensional flows

U. S. Agarwal[a)]
The Dutch Polymer Institute, Faculty of Chemical Engineering, Eindhoven University of Technology, 5600 MB Eindhoven, The Netherlands

(Received 29 November 1999; accepted 24 May 2000)

Brownian dynamics simulations are used to study the unraveling process of polymer molecules in dilute solutions under strong elongational flows. We follow chain extension, segmental alignment, and viscosity contribution behavior of individual, randomly coiled, freely jointed bead–rod chain model molecules. In the absence of hydrodynamic shielding, segmental orientation at an intermediate strain rate begins only when aided by overall chain extension. However, at a very high strain rate, rapid initial segmental orientation and lateral chain compression precedes overall chain extension, resulting in the formation of sharp folds in most chains. Fold formation during the extension process is characterized by a sudden decrease in the rate of overall chain extension, an intermediate plateau in birefringence, and a disproportionately low chain end-to-end distance. Hydrodynamic screening generally slows down the uncoiling process, sometimes enough to avoid the formation of folded conformations. © *2000 American Institute of Physics.* [S0021-9606(00)50932-5]

I. INTRODUCTION

In the absence of any external forces, a polymer chain in solution stays randomly coiled due to Brownian motion. Under sufficiently strong flow conditions, the solvent drag force causes extension of the polymer molecule.[1,2] The drag force on an initially coiled macromolecule increases as it unravels, and it uncoils abruptly[1–4] if the strain rate ($\dot{\epsilon}$) exceeds a critical value ($\dot{\epsilon}_{cs}$). For a given strain rate, there exists a certain equilibrium level of stretching of a given macromolecule when the Brownian or elastic coiling forces are balanced by the stretching drag forces.

Small quantities of dissolved long chain polymers are used as additives to influence the rheology of liquids. Many rheology modifying applications such as turbulent drag reduction and enhanced oil recovery are based on the flow induced stretching process of dissolved polymer coils, and the influence of the deformed polymer chains on solution rheology. The extent of chain stretching is also important in determining the chain scission tendency during strong flows.[4–7] Extensional flows at ($\dot{\epsilon} > \dot{\epsilon}_{cs}$) often involve the polymer molecules experiencing the stretching forces for a limited time or strain. If this strain is not sufficient for complete stretching of the polymer molecules, then the solution rheology is dependent on the extent and rate of stretching, and hence on the strain history of the solution.[8–11]

Various models (dumbbells, bead–spring or bead–rod chains, etc.) are used to represent polymers, and in each case, predictions about stretching and rheology are made based on calculations of averages.[2] Simulations are often used in the case of more complicated models or flow situations. Many simulations suggest the formation of certain special chain conformations during unraveling of coiled chain polymers. Acierno, Titomantio, and Marrucci[12] observed backloops in their simulations of flowing polymers. King and James[13] observed a substantial increase in extensional viscosity before complete chain extension, and attributed this to freezing of the polymer structure due to self-entanglements in partially extended conformations. Neglecting Brownian motion at high strain rates, Rallison and Hinch[14] observed segmental alignment and multiple fold formation to a highly kinked state, leading to viscous stresses. Ryskin[15] suggested preferential extension of the chain *center* in the initial stages. But Wiest, Wedgewood, and Bird[16] predicted nearly simultaneous orientation of *all* segments in the initial stages, which was followed by unfolding of the chains. Larson[17] presented a kink dynamics model to describe the process. Based on the observed decrease in extensional viscosity with increase in strain rate (at high strain rates) in transient elongational flows, Cathey and Fuller[18] tentatively suggested that for a given total strain, a smaller residence time at higher extension rates was responsible for incomplete chain extension in the limited residence time spent in the flow field. van den Brule[19] and Hinch[20] used Brownian dynamics simulations to follow stretching of polymer chains in strong extensional flows, and found that in the initial stages, *all* segments orient without contributing much to the total viscosity, indicating kinked configurations. Subsequent unfolding resulted in final chain extension. Unfolding of the last few backloops was the slowest.[20] Recently the direct imaging experiments of Smith and co-workers[21,22] clearly demonstrated that different long chain DNA molecules unravel at very different times in the same elongational flow field. They attributed this to formation of fold-prone and dumbbell-prone conformations during initial affine deformation to a fractional stretch of 1/3. The tendency for fold formation was higher at higher strain rates.[22] In their Brownian dynamics simulations, Hernandez Cifre and Garcia de la Torre[23] observed that bead–spring chains underwent stretching along elongational flow direc-

[a)]Electronic mail: u.s.agarwal@TUE.NL

tion at different instants, depending on individual conformations. Recently Larson *et al.*[24] have reported quantitative agreement of their Brownian dynamics simulations with the DNA imaging experiments. They concluded that initial chain conformation is the prime factor that determines the unraveling path of polymer molecules at high strain rates.

In this paper we examine the stretching process of individual molecules, using Brownian dynamics simulations. We focus on ten different individual chains, each with a different initial random coil conformation. We follow not only the overall chain stretching (end-to-end distance, and radius of gyration), but also the segmental alignment (as indicated by flow birefringence) and molecular stresses (as indicated by solution intrinsic viscosity), to enable relation to rheo-optical characteristics. To evaluate the effect of hydrodynamic interaction (HI), we compare the unraveling behavior with and without HI, and at different strain rates.

II. BROWNIAN DYNAMICS SIMULATION

Isolated freely jointed bead–rod model chains consisting of $N=100$ links (each of length l) and $(N+1)$ beads (each of radius a) are used to analyze the behavior of linear polymer molecules in a simple elongational flow field $\mathbf{v}(\mathbf{r})$ given by

$$v_x=\dot{\epsilon}x, \quad v_y=-(\dot{\epsilon}/2)y, \quad v_z=-(\dot{\epsilon}/2)z. \tag{1}$$

Brownian Dynamics simulations are carried out in steps of time Δt, in accordance with the SHAKE-HI algorithm.[25] During any step, the new position vector $\mathbf{r}(t+\Delta t)$ of the ith bead is calculated from the position $\mathbf{r}_i(t)$ at the beginning of the step by

$$\mathbf{r}_i(t+\Delta t)=\mathbf{r}_i(t)+(\Delta t/kT)\sum_j \mathbf{D}_{ij}\mathbf{F}_j+\mathbf{R}_i(\Delta t), \tag{2}$$

where $\mathbf{F}_j$ is the sum of flow drag force and intramolecular (i.e., ''bond'' length constraint) forces acting on bead j at time t. $\mathbf{D}_{ij}$ is the modified Oseen tensor[25,26] accounting for the hydrodynamic interaction between beads i and j. The vector $\mathbf{R}_i$ is the displacement of the ith bead due to Brownian motion, and has a Gaussian distribution with the following properties:

$$\langle \mathbf{R}_i \rangle = 0 \tag{3}$$

and

$$\langle \mathbf{R}_i(\Delta t)\mathbf{R}_j(t+\Delta t)\rangle = 2\mathbf{D}_{ij}\Delta t. \tag{4}$$

We follow chain extension during flow simulations by monitoring the square end-to-end distance (R^2) and radius of gyration (S). R^2 and S are normalized with respect to their full extension value $(Nl)^2$ and $Nl/(2\sqrt{3})$. Thus, the value of normalized $R^{2*}=R^2/(Nl)^2$ varies from $(1/N)=0.01$ for a randomly coiled chain to 1 for a fully stretched chain. Similarly, the value of normalized $S^*=S/(Nl/2\sqrt{3})$ varies from near $\sqrt{(2/N)}\sim 0.14$ for a randomly coiled chain to 1 for a fully stretched chain.

We simultaneously follow the orientation of chain segments along flow direction by monitoring the chain contribution to the birefringence[20] (normalized with respect to its maximum value)

$$\Delta^* = (1/2N)\left(2\sum X_i^2 - \sum Y_i^2 - \sum Z_i^2\right), \tag{5}$$

where X_i and Z_i are the x and z projections of the ith link, and Σ refers to summation over the N links, $i=1,2...,N$.

The contribution of the polymer to the elongational viscosity is determined in terms of the intrinsic viscosity from the Kramers–Kirkwood relation[27]

$$[\eta]=(N_A/\eta_s M\dot{\epsilon})\Big/\sum \langle X_i T_{ix} - Z_i T_{iz}\rangle, \tag{6}$$

where $\mathbf{T}_i$ is the constraint force in the ith link, and is calculated using the Lagrangian constants obtained in the Allison and McCammon algorithm.[25] η and η_s are the viscosities of the solution and the solvent, respectively. The corresponding normalized intrinsic viscosity is obtained as

$$[\eta]^*=[\eta](M/N_A l^3)=(2\pi a^*/\dot{\epsilon}^*)\sum \langle X_i^* T_{ix}^* - Z_i^* T_{iz}^*\rangle, \tag{7}$$

where the projections X_i and Z_i are made dimensionless by dividing by l, the forces by kT/l, time by $\zeta l^2/kT$. $\zeta = 6\pi\eta_s a$ is the bead friction factor. Hereafter in the paper, only the dimensionless quantities are used, and the asterisk (*) is dropped for convenience.

III. SIMULATION METHODOLOGY

Computations are carried out for $N=100$ rod chains. To study the contribution of hydrodynamic interaction, two cases are considered

(i) the free-draining case, i.e., no hydrodynamic interactions, and
(ii) the non-free-draining case, i.e., with hydrodynamic interaction defined by $(a=0.4)$.

For each case, configuration development is followed during simulations carried out at two different strain rates: (i) at an intermediate strain rate $\dot{\epsilon}_1$ near the upper end of the coil–stretch transition region, corresponding to equilibrium mean square end-to-end distance $R^2\sim 0.8$, and (ii) at a much higher strain rate $\dot{\epsilon}_2=0.48$. The values of $\dot{\epsilon}_1$ for these representative simulations are different for the free-draining case $(\dot{\epsilon}_1=0.02)$ and the non-free-draining case $(\dot{\epsilon}_1=0.06)$, because coil–stretch transition behavior is dependent on HI, as seen in the previous paper.[8] The chosen $\dot{\epsilon}_1$ here are much higher than $\dot{\epsilon}_{cs}$ (0.003 and 0.022 for the free-draining and the non-free-draining cases, respectively[8]) because the objective here is to examine the effect of chain folding that hinders the stretching process. The simulations were begun by starting with initially randomly coiled chains that were generated by successively joining 100 links. Each link was of length 1, and was randomly oriented. Ten such chains with different initial conformations were generated using different arbitrary seeds for random number generation. The trajectory simulation was carried out in small time steps given by $\dot{\epsilon}\Delta t = 0.000\,012$, so that the fluid strain contribution was the same in all simulations presented here, even as the strain rates were varied. During the Brownian dynamics simulation of each chain, values R^2, S, Δ, and $[\eta]$ over each 1000 steps

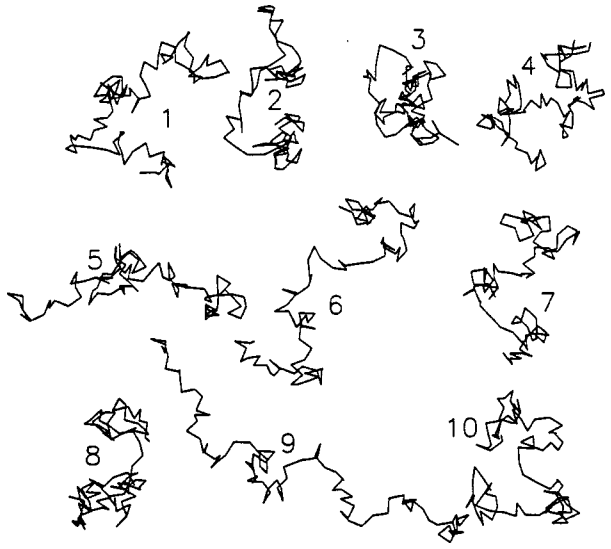

FIG. 1. *XY* projection of ten randomly generated $N=100$ bead–rod chains at $t=0$, $\epsilon=0$. The chains are numbered as shown.

were averaged and then stored as function of time (t) already spent in the flow field. Each trajectory simulation was continued until achieving flattening of these characteristics to corresponding equilibrium values. Only one set of random Gaussian numbers was generated for calculating the corresponding sets of Brownian contributions [R_i in Eq. (2)] according to the SHAKE-HI algorithm.[25] This was used in all simulations reported here, to eliminate any effect of differences in Brownian contributions.

One limitation of the present simulations is that the chain segments are considered to move across each other in a phantom manner, thus perhaps enabling unrealistically easy release of folds.

IV. RESULTS AND DISCUSSIONS

A. Free-draining case

1. Stretching at the intermediate strain rate $\dot{\epsilon}_1$

Figure 1 shows the ten different randomly generated chains at $t=0$. For affine deformation, the Henky strain ($\epsilon=\dot{\epsilon}t$) required for complete stretching at high $\dot{\epsilon}$ is predicted[17,30] to be

$$\epsilon_f = 1 + \ln(\sqrt{N}) = 3.3 \quad \text{for } N = 100. \tag{8}$$

Figure 2 shows the extension process of these chains in a free-draining field extensional field of $\dot{\epsilon}_1=0.02$. We find that different chains undergo stretching at different strains, depending on the initial conformation. For example, chains 9 and 5 undergo very quick stretching, requiring significantly less than 3.3 strain units [Eq. (8)] to achieve the maximum stretching. This is because even though the initial segmental orientation is random, these two chains already have significant overall extension along the flow direction (Fig. 1). As

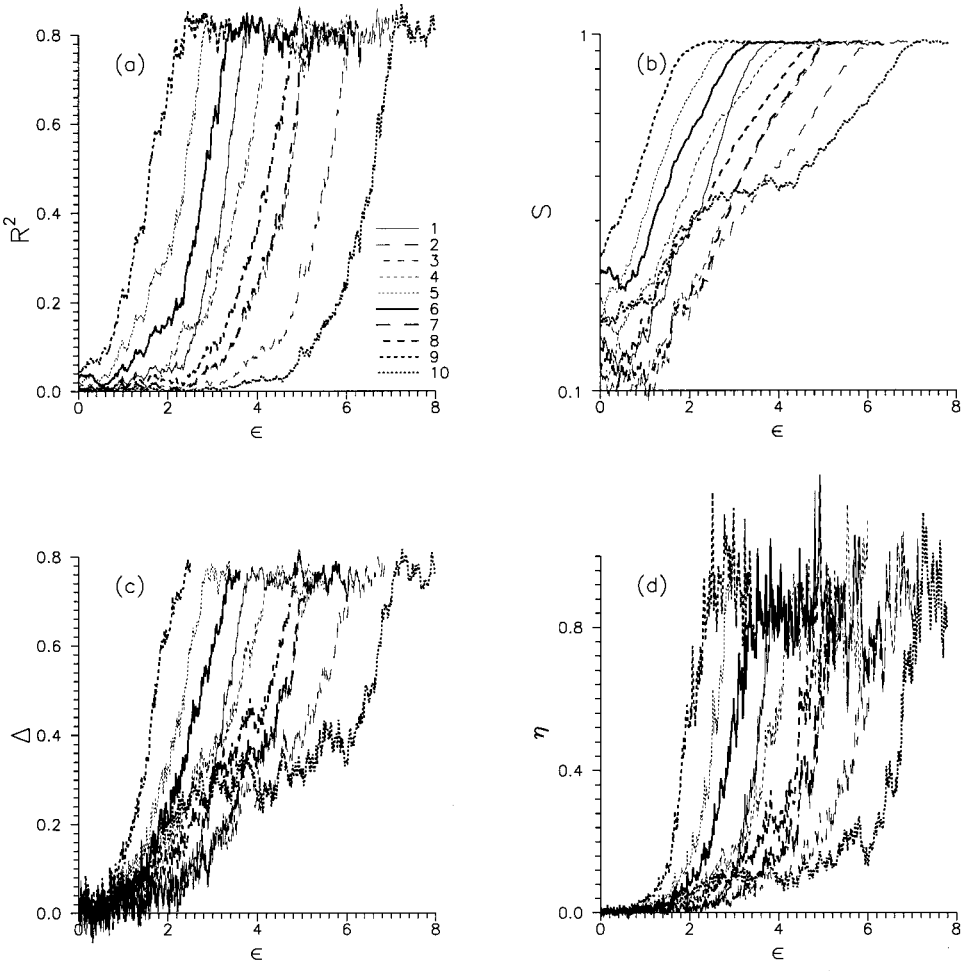

FIG. 2. Increase in (a) R^2, (b) S, (c) Δ, and (d) $[\eta]$ with strain, for chains of Fig. 1 in a free-draining elongational flow field of ($\dot{\epsilon}_1=0.02$). The legend for the chain numbers of the curves is shown in Fig. 2(a), and is the same for all figures.

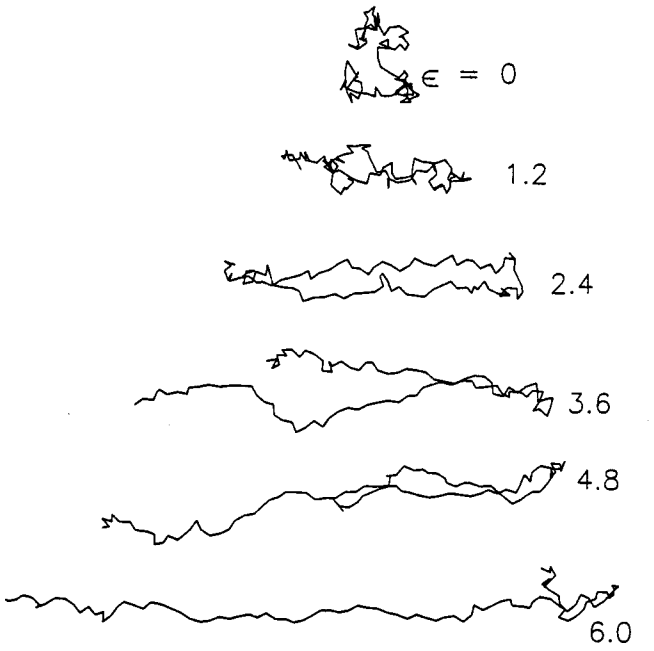

FIG. 3. Snapshots of *XY* projections of chain 10 (Fig. 1) at different strains in the free-draining elongational flow field of ($\dot{\epsilon}_1 = 0.02$).

seen from Fig. 2, these chains begin to stretch as soon as fluid strain is imposed, and the inception time is negligible. Chain 6 also has a large overall initial extension, but not along the flow direction (Fig. 1). Hence it requires an inception time before segmental aligning and overall stretching begins. The overall initial extensions of the other chains are comparable to each other [$S \sim 0.11-0.15$ at $\epsilon = 0$, Fig. 2(b)], and they display inception delay. In the initial stages, an increase in S precedes the increase in Δ, indicating that *segmental* orientation occurs only *after* initial overall chain *extension*. This is because the strain rate is not enough to cause orientation of the chain segments, unless aided by the overall chain stretching.

For chain 10, even though the initial rise in S and Δ (to 0.3) takes place quickly (at $\epsilon \sim 2.5$), significant increase in R^2 occurs only much later ($\epsilon \sim 5$). By plotting its conformations at various strains in Fig. 3, we see that at strain as low as 1.2, the chain compresses in the direction perpendicular to the flow, which results in formation of a fold near the chain center at ($\epsilon \sim 2.4$). As seen from Figs. 1 and 3, initially chain 10 has both its ends *distinctly* on the left-hand side of the molecular center, and is thus susceptible to fold formation.[24] Once a hairpin structure has formed at ($\epsilon \sim 2.4$), unfolding and chain stretching continues (Fig. 3) due to Brownian motion and axial flow, though until $\epsilon \sim 5$ only very slowly [Figs. 2(b) and 2(c), *hesitatingly*[24]]. As we shall see further, the sudden decrease in slope of the $S-\epsilon$ curve, disproportionately small R^2, and an intermediate plateau in the $\Delta-\epsilon$ curve, all simultaneously at ($\epsilon \sim 2.4$) are signatures of fold formation. Beyond ($\epsilon \sim 5$), the chain ends land on opposite sides of the chain center of mass (Fig. 3). As these chain ends now get pulled in opposite directions [Eq. (1)], the subsequent unraveling is faster [Fig. 2(b)]and the chain end-to-end distance also increases rapidly [Fig. 2(a)].

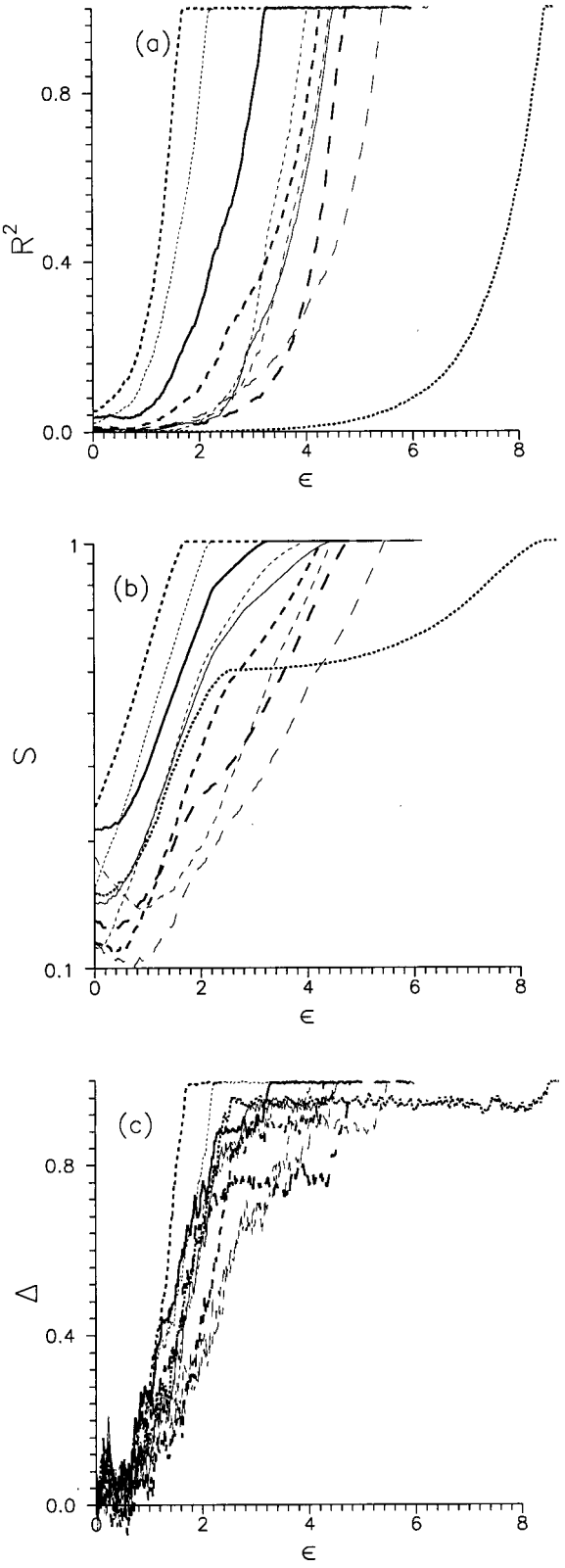

FIG. 4. Increase in (a) R^2, (b) S, and (c) Δ with strain for the chains of Fig. 1 in the free-draining elongational flow field of ($\dot{\epsilon}_2 = 0.48$). The legend is as in Fig. 2(a).

The contributions of various chains to the solution's elongational viscosity are shown in Fig. 2(d). For the quickly unfolding chains 9 and 5, the viscosity rise is more sudden than R^2, S, or Δ increase. This is because the initial unrav-

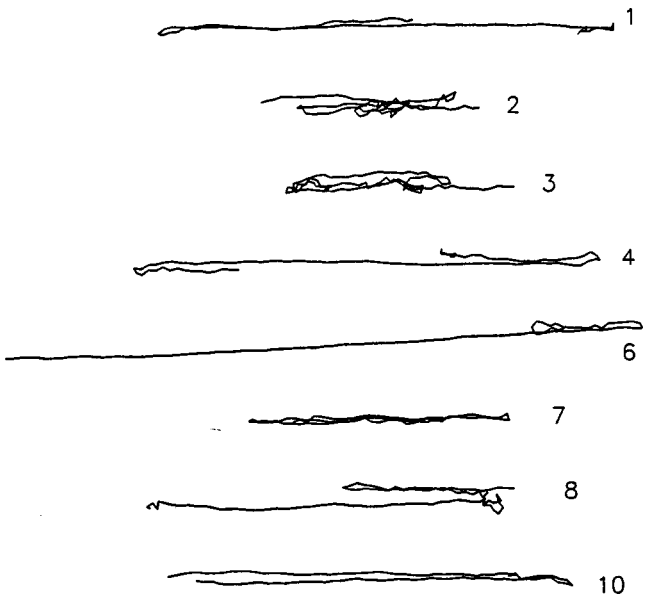

FIG. 5. Snapshots of *XY* projections of the chains of Fig. 1 at strain $\epsilon = 2.4$ in the free-draining elongational flow field of ($\dot{\epsilon}_2 = 0.48$). Chain numbers are shown.

eling of the chains is affine with the solvent deformation, and hence little dissipation occurs, resulting in only a small contribution of the polymer to the solution viscosity.[14,20] As the chain stretching saturates to equilibrium value, segmental motion cannot keep up with fluid strain, and dissipation and viscosity increase suddenly. For chain 10, the intermediate fold formation results in an intermediate, temporarily *hung up*[24] structure. Slower than affine deformation (not quite ''frozen'') in this substantially extended structure causes some energy dissipation,[14,19] thereby contributing to solution viscosity ($[\eta] \sim 0.1$).

2. Effect of strain rate

Similar results at the higher strain rate ($\dot{\epsilon}_2 = 0.48$) are shown in Fig. 4. The dependence on the initial chain conformation is largely similar to the behavior at $\dot{\epsilon}_1$, i.e., chains 9 and 5 undergo quick unraveling, while chain 10 undergoes intermediate fold formation (as reflected in the signatures, i.e., a sudden decrease in slope of $S-\epsilon$, disproportionately small R, and an intermediate plateau in $\Delta-\epsilon$) at ($\epsilon \sim 2.4$), although with a much higher segmental alignment in the folded state ($\Delta \sim 0.97$). From Fig. 4(c), we observe that variation in Δ rise behavior of different chains is small in the early stages. For example, $\Delta \sim 0.6$ is achieved by all chains in a narrow range of strains 1.5–2.4 units. This indicates that at such high strain rate ($\dot{\epsilon}_2$), the initial *segmental* alignment is quick and has only a weak dependence on the initial chain conformation. However, the overall chain extension [Fig. 4(b)] is strongly affected by the initial molecular conformation even at $\dot{\epsilon}_2$. This extension is rapid (without inception delay) for the facile chains 9 and 5. But for all other chains, extension is slowed down by formation of sharp folds (Fig. 5).

Thus, at the very high strain rates such as $\dot{\epsilon}_2$, the tendency for fold formation can be very high, as also observed

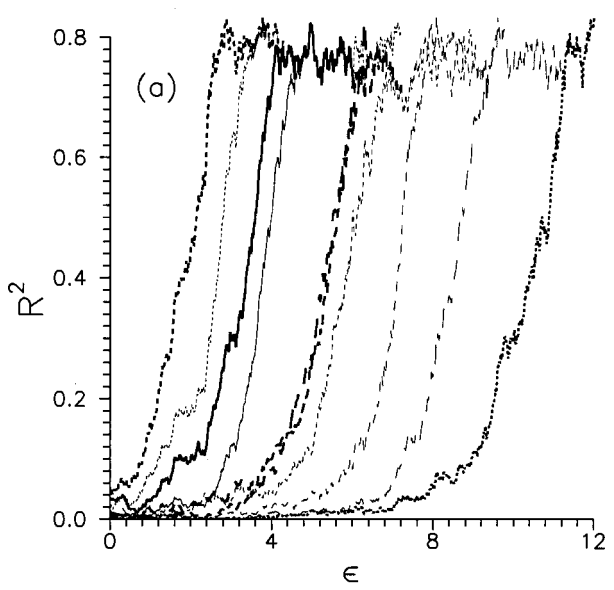

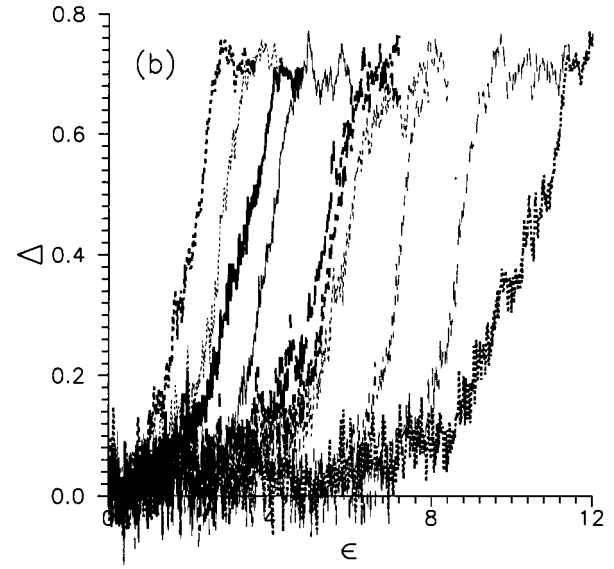

FIG. 6. Increase in (a) R^2 and (b) Δ with strain, for the chains of Fig. 1 in a non-free-draining elongational flow field of ($\dot{\epsilon}_1 = 0.06$). The legend is as in Fig. 2(a).

by Larson *et al.*[24] Here we attribute this to the quick ($\epsilon \sim 2-3$) segmental alignment and lateral compression of the chain segments, before significant chain stretching along flow can occur. In contrast, the segmental alignment and lateral compression are reduced at the lower strain rate. Further, the time required for the same strain is more and hence the Brownian motion makes a sufficient contribution to allow the release of ''potential'' folds. We expect that for a given flow field, an increase in solvent viscosity would increase flow drag in comparison to Brownian motion, and thus enhance the chain folding tendency.

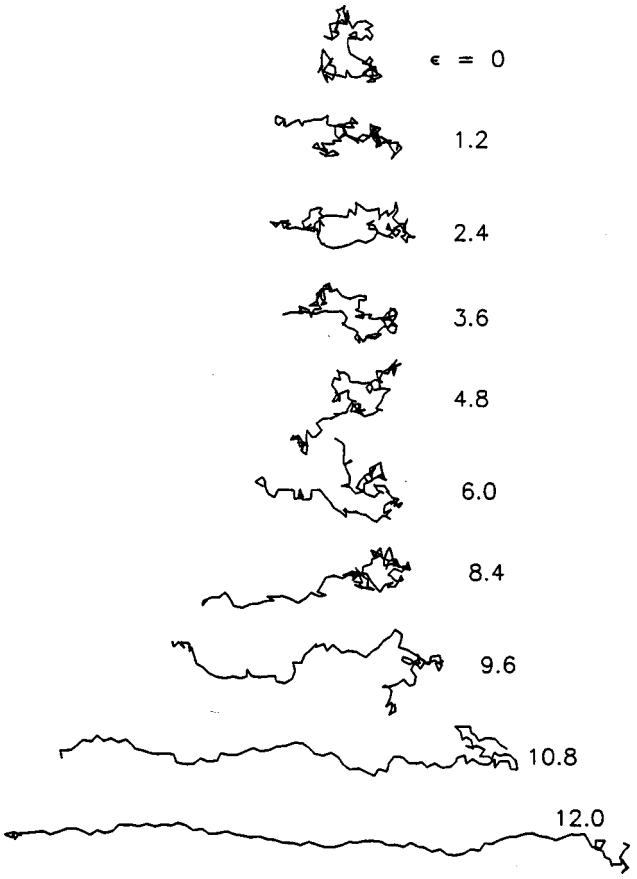

FIG. 7. Snapshots of *XY* projections of chain 10 (Fig. 1) at different strains in the non-free-draining elongational flow field of ($\dot{\epsilon}_1 = 0.06$).

B. Non-free-draining case

1. Effect of HI at the intermediate strain rate $\dot{\epsilon}_1$

The uncoiling processes of the ten different chains in a non-free-draining extensional field at $\dot{\epsilon}_1$ are shown in Fig. 6. We again find a wide distribution of strains over which the different chains get extended. We find that an increase in Δ and R^2 correspond to each other quite well *throughout* the stretching process of all chains, and we see no intermediate plateau in Δ rise behavior. This is in contrast to the no-HI situation at $\dot{\epsilon}_1$ [Fig. 2(a)] where a quick initial rise in Δ for all chains was observed at ($\epsilon < 4$), and for chain 10, a fold indicating intermediate plateau in Δ was observed. In the HI case, even though rapid overall chain compression takes place in the direction perpendicular to flow (such as for chain 10, Fig. 7, $\epsilon = 1.2$), the Δ rise does not even *begin* for six of the chains at $\epsilon = 4$ [Fig. 6(b)], and in general the chain extension requires larger strains Figs. 2(a) and 6(a)]. Longer inception strain for unraveling of most chains with HI was also observed by Hernandez Cifre and Garcia de la Torre,[23] and we here explore the details. This delay is caused by the beads of the coiled chain (compressed to somewhat uniaxial shape) being shielded from the axial drag of bulk fluid flow, due to the presence of other beads in the neighborhood (along streamline). Stretching of the collapsed chain finally occurs due to Brownian diffusion induced fluctuations (expansion[8,28,29]) leading to a reduction in hydrodynamic shielding. Once such unfolding begins, it proceeds for all

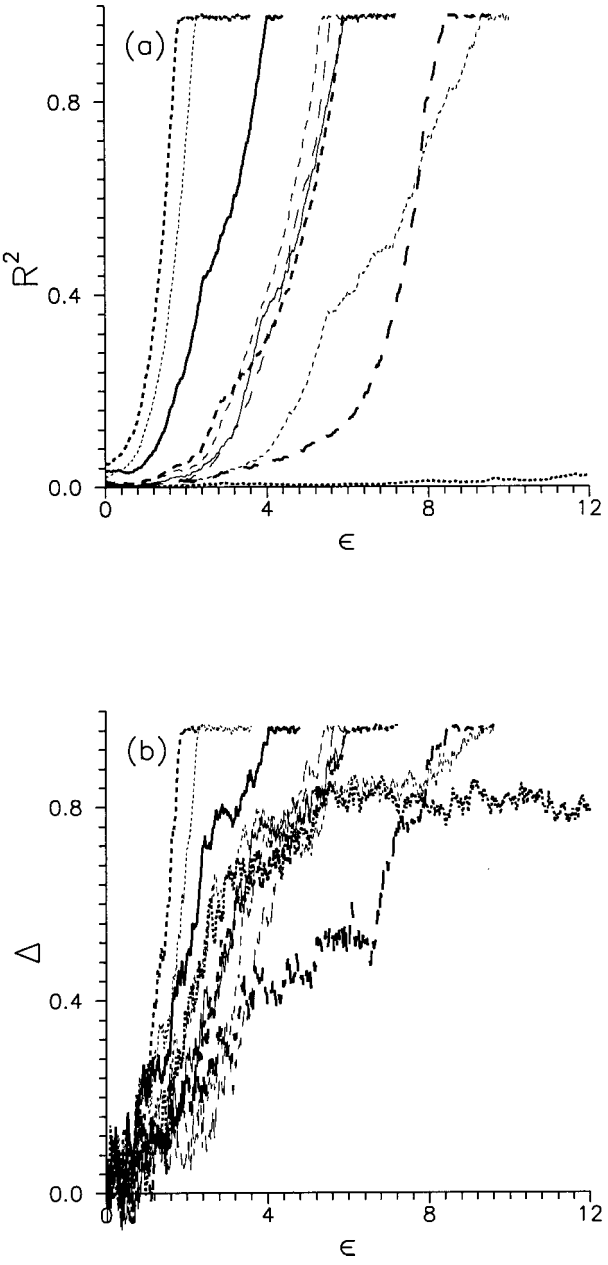

FIG. 8. Increase in (a) R^2 and (b) Δ with strain, for the chains of Fig. 1 in a non-free-draining elongational flow field of ($\dot{\epsilon}_2 = 0.48$). The legend is as in Fig. 2(a). Chain 10 requires $\epsilon \sim 25$ for complete stretching.

cases (including chain 10) without any intermediate plateau in Δ, and at increasing rate (Fig. 7), unlike the ''hesitating'' linear increase in the no-HI case (Fig. 3). Thus, the very nature of unraveling behavior of fold-prone chains at this intermediate strain rate is strongly influenced by HI. There is a longer inception delay, and during this time the fold forming tendency is reduced perhaps due to the longer time available for Brownian fluctuations to eliminate potential folds.

2. Effect of HI at the higher strain rate $\dot{\epsilon}_2$

Results for the stretching behavior at $\dot{\epsilon}_2 = 0.48$ are shown in Fig. 8. The dependence on the initial chain conformation is largely similar to the behavior for the no-HI case at the same $\dot{\epsilon}_2$ (Fig. 4), i.e., different times for unraveling,

quick unraveling of chains 5 and 9, slow R^2 rise for most others in spite of the quick initial rise in Δ for all chains in a narrow range of strains, the presence of intermediate plateau in Δ curves for many chains (1, 3, 4, 6, 7, 8, and 10), and large differences in Δ rise behavior beyond the plateau formation. Unraveling of the compact coil fold-prone conformations at $\dot{\epsilon}_2$ is delayed by HI (Figs. 4 and 8), as was observed at $\dot{\epsilon}_1$ (Figs. 2 and 6). However, unraveling of chains 9 and 5 at $\dot{\epsilon}_2$ requires the same strain in the presence of HI (Fig. 8) as in the no-HI case (Fig. 4). This indicates that for the sufficiently expanded conformations, hydrodynamic shielding is not strong enough to significantly reduce the flow drag (or to slow down the chain extension) at such high strain rates.

3. Effect of strain rate in the presence of HI

Similar to the no-HI case, the higher strain rate also increases the fold-forming tendency in the HI case. In the region of onset of coil–stretch transition, the average strain required for chain stretching decreases [before leveling out to the prediction of Eq. (8)] with increase in strain rate, due to the smaller relative contribution of Brownian fluctuations.[8,28,29] Comparing Figs. 6(a) and 8(a), we find that most fold forming chains (i.e., other than chains 9 and 5), with the exception of chain 3, require higher strains for stretching at the higher strain rate [Figs. 6(a) and 8(a)]. This may be because of the stronger HI shielding effect as the two arms of the folded chain are aligned along each other closely at the higher strain rate. Thus, for a given strain, a higher strain rate may result in smaller chain extension and hence a decrease in viscosity contribution. James and Sridhar[30] in fact observed a decrease in dilute solution elongational viscosity at very high strain rate, though they believed it to be due to self-entanglements limiting the molecular extension.

V. CONCLUSIONS

Results are presented for Brownian dynamics simulations of phantom polymers in elongational flow fields of intermediate strength ($\dot{\epsilon}_1$, above coil–stretch transition) and very high strength ($\dot{\epsilon}_2$). In all cases, the initial chain conformation has a strong influence on the overall chain extension. In the absence of HI, at $\dot{\epsilon}_1$, the segmental alignment follows overall chain extension as the former needs to be aided by the latter at this strain rate. At very high strain rates such as $\dot{\epsilon}_2$, the initial segmental alignment is independent of the chain conformation, and precedes overall chain extension. The flow field [Eq. (1)]causes quick chain compression lateral to the flow, and thus fold formation in most chains at 2–3 strain units. Fold formation is characterized by a sudden decrease in the rate of S rise, intermediate plateau in Δ, and a disproportionately low R^2. Further extension of the folded conformations proceeds slowly, and this *rigidity* makes a small contribution to solution viscosity.

HI generally delays the onset of the stretching process as the segments in the compressed chain are somewhat shielded from the axial flow. At $\dot{\epsilon}_1$, the segmental alignment is also delayed, and finally occurs together with overall chain extension. The delay may allow enough time for Brownian fluctuations to reduce fold forming tendency. At the higher strain rate, the delaying effect of shielding is seen primarily in compact coil, fold forming chains.

[1] A. Peterlin, Pure Appl. Chem. **12**, 563 (1966).
[2] R. B. Bird, C. F. Curtiss, R. C. Armstrong, and O. Hassager, *Dynamics of Polymeric Fluids*, Kinetic Theory Vol. 2 (Wiley, New York, 1987).
[3] P. G. DeGennes, J. Chem. Phys. **60**, 5030 (1974).
[4] J. A. Odell and A. Keller, J. Polym. Sci., Polym. Phys. Ed. **24**, 1889 (1986).
[5] T. Q. Nguyen and H. H. Kausch, Adv. Polym. Sci. **100**, 73 (1992).
[6] U. S. Agarwal and R. A. Mashelkar, J. Chem. Phys. **100**, 6055 (1994).
[7] U. S. Agarwal and R. A. Mashelkar, J. Non-Newtonian Fluid Mech. **54**, 1 (1994).
[8] U. S. Agarwal, R. Bhargava, and R. A. Mashelkar, J. Chem. Phys. **108**, 1610 (1998).
[9] D. F. James, B. D. McLean, and J. H. Saringer, J. Rheol. **31**, 453 (1987).
[10] A. M. Wunderlich and D. F. James, Rheol. Acta **26**, 522 (1987).
[11] K. Vissmann and H.-W. Bewersdorff, J. Non-Newtonian Fluid Mech. **34**, 289 (1990).
[12] D. Acierno, G. Titomantio, and G. Marrucci, J. Polym. Sci., Polym. Phys. Ed. **12**, 2177 (1974).
[13] D. H. King and D. F. James, J. Chem. Phys. **78**, 4749 (1983).
[14] J. M. Rallison and E. J. Hinch, J. Non-Newtonian Fluid Mech. **29**, 37 (1988).
[15] G. Ryskin, J. Fluid Mech. **178**, 423 (1987).
[16] J. M. Wiest, L. E. Wedgewood, and R. B. Bird, J. Chem. Phys. **90**, 587 (1989).
[17] R. G. Larson, Rheol. Acta **29**, 371 (1990).
[18] C. A. Cathey and G. G. Fuller, J. Non-Newtonian Fluid Mech. **34**, 63 (1990).
[19] B. H. A. A. van den Brule, J. Non-Newtonian Fluid Mech. **47**, 357 (1993).
[20] E. J. Hinch, J. Non-Newtonian Fluid Mech. **54**, 209 (1994).
[21] D. E. Smith and S. Chu, Science **281**, 1335 (1998).
[22] D. E. Smith, H. P. Babcock, and S. Chu, Science **283**, 1724 (1999).
[23] J. G. Hernandez Cifre and J. Garcia de la Torre, J. Non-Cryst. Solids **235–237**, 717 (1998).
[24] R. G. Larson, H. Hu, D. E. Smith, and S. Chu, J. Rheol. **43**, 267 (1999).
[25] S. A. Allison and J. A. McCammon, Biopolymers **23**, 167 (1984).
[26] J. Rotne and S. Prager, J. Chem. Phys. **50**, 4831 (1969); H. Yamakawa, *ibid.* **53**, 436 (1970).
[27] J. G. Kirkwood and J. Riseman, J. Chem. Phys. **14**, 415 (1948).
[28] J. J. Magda, R. G. Larson, and M. E. Mackay, J. Chem. Phys. **89**, 2504 (1988).
[29] R. G. Larson and J. J. Magda, Macromolecules **22**, 3004 (1989).
[30] D. F. James and T. Sridhar, J. Rheol. **39**, 713 (1995).